AIAA JOURNAL
Vol. 39, No. 11, November 2001

Coupled Analytical Sensitivity Analysis and Optimization of Three-Dimensional Nonlinear Aeroelastic Systems

K. Maute,* M. Nikbay,† and C. Farhat‡
University of Colorado, Boulder, Colorado 80309-0429

We consider the problem of optimizing for steady-state conditions a given nonlinear aeroelastic system, by varying both aerodynamic and structural parameters. We model the structure by finite elements and predict the aerodynamic loads by a three-dimensional finite volume approximation of the Euler equations. We present a complete optimization methodology whose key components are a computer aided geometric design method for representing the design, an analytical approach for sensitivity analysis, a gradient-based optimization algorithm and two staggered schemes for evaluating the aeroelastic responses and solving the coupled sensitivity equations. We illustrate our methodology and demonstrate its potential with various aeroelastic optimizations of idealized and builtup wing structures.

I. Introduction

TODAY, the design of complex aeronautical systems remains a challenging task because it must account for several nonlinear fluid, structure, and thermal coupling effects. Although for such systems intuition, experience, and engineering skills still dominate the design process, numerical simulation offers an important potential for speeding up the design cycle.

In general, a design problem is defined in terms of physical design parameters, objectives to be optimized, and constraints to be satisfied. Typically, the objectives and constraints are functions of the system's response, which in turn is governed by a set of coupled partial differential equations that describe the various physical effects and their coupling. However, because of complexity and computational cost issues, most often the coupling effects are neglected when developing an optimization method or applying it to a practical system. For example, in conventional structural optimization, the dependence of a fluid-induced structural load on a given optimization criterion is typically ignored, and in conventional aerodynamics optimization, the structure is assumed to be rigid and the various optimization criteria cover only the flow characteristics. For a survey of structural optimization, see, for example, Kirsch[1] and Bendsøe[2]; and for a survey of aerodynamic optimization, see Newman et al.[3] and Jameson.[4] Nevertheless, because the overall performance of an aeronautical system is governed in many cases by coupling effects, multidisciplinary optimization methods in general, and aeroelastic optimization algorithms in particular, have flourished in recent years.

For practical reasons, simple structural models and linear flow theories have dominated the field of aeroelastic optimization (for example, see Refs. 5–8). However, with the availability of ever faster computing platforms and the advent of parallel processing, detailed finite element structural models and nonlinear flow theories have made their way into the aeroelastic optimization process. For example, Giunta and Sobieszczanski-Sobieski[9] have performed the aeroelastic optimization of a supersonic aircraft design by coupling a linear finite element code for the structure and an Euler code for the fluid. However, their approach is computationally intensive because it relies on a finite difference scheme for evaluating the gradients of the optimization criteria. To lower the computational requirements, Giunta[10] introduced a reduced structural model for the fluid/structure coupling. However, such an approach can induce relative errors for the aeroelastic sensitivities that exceed 25% (Ref. 10) and, therefore, is not a reliable methodology.

The shortcomings of finite differencing for sensitivity analysis are usually overcome by an analytical evaluation of the sought-after gradients. However, for multidisciplinary problems in general and aeroelasticity in particular, the analytical approach imposes special requirements on the fluid and structural analyzers and calls for the solution of yet another complex system of coupled fluid/structure equations. Ghattas and Li[11] and Møller and Lund[12] have addressed this issue in the two-dimensional case, and Maute et al.,[13] as well as Hou and Satyanarayana,[14] have addressed it in the three-dimensional context.

In this paper, we build on the preliminary work exposed in Ref. 13 and present a methodology for optimizing realistic aeroelastic systems that is based on coupled analytical sensitivities. We consider the case where the structure is represented by a detailed finite element model and the fluid by the three-dimensional Euler equations. Our overall methodology is based on a modular framework for formulating and solving the target optimization problem. Its key components are a comprehensive three-field formulation of an aeroelastic system and fast parallel staggered algorithms for evaluating the aeroelastic responses and computing the analytically derived gradients of the optimization criteria.

The remainder of this paper is organized as follows. In Sec. II, we formulate the aeroelastic optimization problem and present a three-level modular approach for solving it. In Sec. III, we overview the three-field representation of the aeroelastic problem and summarize the numerical procedure adopted for evaluating the design criteria. In Sec. IV, we describe the global sensitivity equations for the aeroelastic problem described by the three-field formulation and derive the corresponding direct and adjoint solution approaches. We also present and discuss a staggered procedure for computing the aeroelastic sensitivities associated with the direct approach. In Sec. V, we investigate the accuracy and performance of the proposed sensitivity analysis and illustrate our methodology with the aeroelastic optimization for steady-state conditions of flat and builtup wing structures. We consider optimization criteria and optimization variables that span lift, drag, structural weight, structural displacements and stresses, orientation of the fibers in composite structural elements, as well as the shape of the dry and wet surfaces.

II. Aeroelastic Optimization

A generic optimization problem associated with a given system can be formulated as

$$\min_{\boldsymbol{s}} z(\boldsymbol{s}) \tag{1}$$

$$\boldsymbol{h}(\boldsymbol{s}) = \boldsymbol{0}, \qquad \boldsymbol{h} \in \mathbb{R}^{n_h} \tag{2}$$

Received 30 November 2000; revision received 20 April 2001; accepted for publication 31 May 2001.

*Assistant Professor, Department for Aerospace Engineering Sciences and Center for Aerospace Structures.

†Research Assistant, Department for Aerospace Engineering Sciences and Center for Aerospace Structures.

‡Professor, Department for Aerospace Engineering Sciences and Center for Aerospace Structures. Fellow AIAA.

$$\boldsymbol{g}(\boldsymbol{s}) \geq \boldsymbol{0}, \qquad \boldsymbol{g} \in \mathbb{R}^{n_g} \tag{3}$$

$$\boldsymbol{s} = \{\boldsymbol{s} \in \mathbb{R}^{n_s} | \boldsymbol{s}_L \leq \boldsymbol{s} \leq \boldsymbol{s}_U\} \tag{4}$$

where $\boldsymbol{s}$ is a set of n_s abstract parameters restricted by lower and upper bounds $\boldsymbol{s}_L$ and $\boldsymbol{s}_U$, z is a cost function of interest, $\boldsymbol{h}$ is a set of n_h equality constraints, and $\boldsymbol{g}$ is a set of n_g inequality constraints.

The physical design parameters can be defined as functions of the abstract optimization variables $\boldsymbol{s}$. For aeroelastic optimization problems, the structural and aerodynamic design parameters can cover, among others, the cross-sectional and thickness dimensions of the structural elements, the shape of the dry and wet surfaces, and the Mach number and angles of attack.

The optimization criteria $\boldsymbol{q}$, that is, the objective function z and the constraints $\boldsymbol{h}$ and $\boldsymbol{g}$, can cover the aerodynamic performance factors such as the lift and drag, as well as the structural behavior descriptors such as the displacements, stresses, and strains. In general, the optimization criteria $\boldsymbol{q}$ depend on the aeroelastic response of the system characterized by the structural displacement vector $\boldsymbol{u}$ and the fluid state vector $\boldsymbol{w}$, which in turn are functions of the physical design parameters, or rather the abstract optimization variables $\boldsymbol{s}$. Therefore,

$$\boldsymbol{q} = \boldsymbol{q}(\boldsymbol{s}, \boldsymbol{u}, \boldsymbol{w}) \tag{5}$$

$$\boldsymbol{u} = \boldsymbol{u}(\boldsymbol{s}), \qquad \boldsymbol{w} = \boldsymbol{w}(\boldsymbol{s}) \tag{6}$$

In this work, we follow the nested analysis and design approach and assume that $\boldsymbol{u}$ and $\boldsymbol{w}$ always satisfy the aeroelastic state equations. For this reason, we do not include the aeroelastic state equations in the set of equality constraints (2), but determine the structural displacements $\boldsymbol{u}$ and fluid state variables $\boldsymbol{w}$ at each iteration of the optimization process.

The aeroelastic optimization problem just described can be solved by combining three different numerical models, namely, the optimization, design, and analysis models (for example, see Maute et al.[15]).

1) In the optimization model, the generic problem (1–4) is solved by a numerical optimization algorithm (for example, see Gill et al.[16] and Vanderplaats[17]). Here, we choose for this purpose a sequential quadratic programming (SQP) algorithm that has demonstrated robustness and efficiency for a broad range of optimization problems.[18] We overview this algorithm in Sec. II.A but refer the reader to Schittkowski[19] and Gill et al.,[20] among others, for further details.

2) In the design model, a shape, or structural, or material, or aerodynamic design parameter is defined as a function of a set of abstract optimization variables. The rationale for such an approach is outlined in Sec. II.B.

3) In the analysis model, the optimization criteria are evaluated. Because these depend in general on the structural and fluid state variables $\boldsymbol{u}$ and $\boldsymbol{w}$, each design in the optimization process $\boldsymbol{u}$ and $\boldsymbol{w}$ calls for the solution of the coupled aeroelastic state equations. The sensitivity analysis is also assigned to this model because it, too, requires the solution of coupled fluid/structure equations. Aeroelastic analysis and sensitivity analyses are discussed in Secs. III and IV, respectively.

A. Optimization Model

It is well known, at least for single-discipline applications, that the generic optimization problem (1–4) can be solved efficiently by gradient-based methods, which are divided into primal, dual, penalty–barrier, and Lagrange approaches. In recent years, Lagrange methods have been shown to be robust and efficient for a broad range of problems in structural optimization.[18] These methods convert the constrained optimization problem (1–4) into that of finding the extremum point of the following Lagrangian:

$$L(\boldsymbol{s}, \boldsymbol{\eta}, \boldsymbol{\gamma}) = z(\boldsymbol{s}) + \boldsymbol{\eta}^t \boldsymbol{h}(\boldsymbol{s}) + \boldsymbol{\gamma}^t \boldsymbol{g}(\boldsymbol{s}) \tag{7}$$

where $\boldsymbol{\eta}$ and $\boldsymbol{\gamma}$ are Lagrange multipliers and, therefore, dual variables of $\boldsymbol{s}$, and the t superscript designates the transpose operation. More specifically, the solution of the original optimization problem (1–4) is in fact the saddle-point of the preceding Lagrangian and, therefore, is the solution of the following Kuhn–Tucker conditions:

$$\frac{\partial L}{\partial \boldsymbol{s}} = \frac{\partial z}{\partial \boldsymbol{s}} + \boldsymbol{\eta}^t \frac{\partial \boldsymbol{h}}{\partial \boldsymbol{s}} + \boldsymbol{\gamma}^t \frac{\partial \boldsymbol{g}}{\partial \boldsymbol{s}} = \boldsymbol{0} \tag{8}$$

$$\frac{\partial L}{\partial \boldsymbol{\eta}} = \boldsymbol{h} = \boldsymbol{0} \tag{9}$$

$$\frac{\partial L}{\partial \boldsymbol{\gamma}} \rightarrow \boldsymbol{\gamma}^t \boldsymbol{g} = \boldsymbol{0}, \qquad \boldsymbol{\gamma} \geq \boldsymbol{0} \tag{10}$$

An SQP method for solving these equations can be described as an extended Newton–Raphson algorithm that incurs at each step the solution of a system of equations of the form

$$\begin{bmatrix} \dfrac{\partial^2 L}{\partial \boldsymbol{s}^2}^{(k)} & \dfrac{\partial \boldsymbol{g}}{\partial \boldsymbol{s}}^{(k)} & \dfrac{\partial \boldsymbol{h}}{\partial \boldsymbol{s}}^{(k)} \\ \boldsymbol{\gamma}^{(k)t} \dfrac{\partial \boldsymbol{g}}{\partial \boldsymbol{s}}^{(k)} & \boldsymbol{g}^{(k)} & \boldsymbol{0} \\ \dfrac{\partial \boldsymbol{h}}{\partial \boldsymbol{s}}^{(k)} & \boldsymbol{0} & \boldsymbol{0} \end{bmatrix} \begin{bmatrix} \Delta \boldsymbol{s}^{(k)} \\ \Delta \boldsymbol{\gamma}^{(k)} \\ \Delta \boldsymbol{\eta}^{(k)} \end{bmatrix} = - \begin{bmatrix} \dfrac{\partial L}{\partial \boldsymbol{s}}^{(k)} \\ \boldsymbol{\gamma}^{(k)t} \boldsymbol{g}^{(k)} \\ \boldsymbol{h}^{(k)} \end{bmatrix} \tag{11}$$

where

$$\Delta \boldsymbol{s}^{(k)} = \boldsymbol{s}^{(k+1)} - \boldsymbol{s}^{(k)}, \qquad \Delta \boldsymbol{\gamma}^{(k)} = \boldsymbol{\gamma}^{(k+1)} - \boldsymbol{\gamma}^{(k)}$$
$$\Delta \boldsymbol{\eta}^{(k)} = \boldsymbol{\eta}^{(k+1)} - \boldsymbol{\eta}^{(k)} \tag{12}$$

and the superscript (k) denotes the iteration index in the optimization loop. The solution of the system of linear equations (11) is also the solution of the quadratic minimization problem:

$$\min_{\boldsymbol{s}} \frac{1}{2} \Delta \boldsymbol{s}^{(k)\,T} \frac{\partial^2 L}{\partial \boldsymbol{s}^2}^{(k)} \Delta \boldsymbol{s}^{(k)} + \frac{\partial z}{\partial \boldsymbol{s}}^{(k)} \Delta \boldsymbol{s}^{(k)} \tag{13}$$

$$\frac{\partial \boldsymbol{g}}{\partial \boldsymbol{s}}^{(k)} \Delta \boldsymbol{s}^{(k)} + \boldsymbol{g}^{(k)} \geq \boldsymbol{0} \tag{14}$$

$$\frac{\partial \boldsymbol{h}}{\partial \boldsymbol{s}}^{(k)} \Delta \boldsymbol{s}^{(k)} + \boldsymbol{h}^{(k)} = \boldsymbol{0} \tag{15}$$

and, therefore, can be efficiently obtained by a quadratic programming method (for example, see Gill et al.[20]) Note that the preceding quadratic subproblem is formulated and solved in each iteration step.

The evaluation of the second derivatives of the optimization criteria being a complex operation, the Hessian of L is usually approximated by a first-order information, for example, by the Davidon–Fletcher–Powell (DFP) or Broyden–Fletcher–Goldfarb–Shanno (BFGS) method (see Ref. 21). However, such an approximation may lead to an incorrect increment $\Delta(\cdot)$. For this reason, the following correction is introduced:

$$\begin{bmatrix} \boldsymbol{s}^{(k+1)} \\ \boldsymbol{\gamma}^{(k+1)} \\ \boldsymbol{\eta}^{(k+1)} \end{bmatrix} = \begin{bmatrix} \boldsymbol{s}^{(k)} \\ \boldsymbol{\gamma}^{(k)} \\ \boldsymbol{\eta}^{(k)} \end{bmatrix} + \alpha^{(k)} \begin{bmatrix} \Delta \boldsymbol{s}^{(k)} \\ \Delta \boldsymbol{\gamma}^{(k)} \\ \Delta \boldsymbol{\eta}^{(k)} \end{bmatrix} \tag{16}$$

and the step size $\alpha^{(k)}$ is determined by a line search. Because the Lagrangian cannot be used to measure an improvement due to Eq. (16), a merit function is introduced and minimized by the line search. Reaching a local optimum is guaranteed by following a sequence of decreasing merit function values. The convergence of the optimization process is measured by the L_2 norm of the residual of the Kuhn–Tucker conditions (8–10). Note that by construction of the solution procedure described herein, the constraints are satisfied only when the optimum point is reached.

B. Design Model

The design model provides an interface between the described optimization model and the analysis model. In general, the relation

between the physical design parameters $\boldsymbol{d}$ and the abstract optimization variables is given by

$$\boldsymbol{d} = \boldsymbol{d}(\boldsymbol{s}), \qquad \boldsymbol{d} \in \mathbb{R}^{n_d} \tag{17}$$

where n_d is the number of physical design parameters. A structural or aerodynamic parameter may be directly identified with an abstract optimization variable, in which case $d_j = s_i$. This is the case, for example, if an abstract optimization variable represents the freestream Mach number. However, the relation between the abstract and physical parameters can be more complex, for example, when the shape of the structure or the boundary of the fluid domain is a design variable. In such cases that usually pertain to shape optimization, the following design model is introduced to define a relation between the abstract optimization variables and the motion $\boldsymbol{x}$ of the nodes of the structure and/or fluid meshes:

$$\boldsymbol{x} = \boldsymbol{x}(\boldsymbol{s}) \tag{18}$$

A direct approach is to identify an abstract optimization variable with an increment of the coordinate of a grid point on the structural boundaries.[22] However, this can lead to irregular shapes because of numerical instabilities. For example, finite elements are in general sensitive to geometrical distortions that may produce artificial stiffening.[23] For this and other reasons, a generic design model is necessary in practice.

Two approaches, namely, mechanical and geometrical, can be adopted for constructing a generic design model. In the mechanical-based approach, the shape variation is identified with a superposition of fictitious structural deformations $\bar{\boldsymbol{u}}_j$ due to fictitious loads $\mu_j \bar{\boldsymbol{P}}_j$ and fictitious support conditions (for example, see Belegundu and Rajan[24]):

$$\boldsymbol{x} = \sum_j \bar{\boldsymbol{u}}_j = \sum_j \bar{\boldsymbol{K}}_j^{-1} \mu_j \bar{\boldsymbol{P}}_j \tag{19}$$

where $\bar{\boldsymbol{K}}_j$ is the stiffness matrix of the real structure or a fictitious structure representing the fluid domain for the current fictitious support conditions. For each fictitious load case, the load factor μ_j is varied, so that μ_j can be identified with the abstract optimization variable s_i.

In the geometrical approach, the geometry of the structure or the fluid boundaries is described by means of computer-aided geometric design methods such as solid modeling or the design element concept.[25,26] In the design element concept, the shape of a body $\boldsymbol{X}$ is approximated piecewise by the so-called design elements as follows:

$$\boldsymbol{X} = \sum_j \Phi_j(\xi) \hat{\boldsymbol{X}}_j \tag{20}$$

where Φ_j is a shape function, $\hat{\boldsymbol{X}}_j$ the vector of control nodes, and ξ the elemental coordinate system. Frequently used design elements are Lagrange and Bézier curves as well as B-spline and NURBS for edges; surfaces can be described by Lagrange, Bézier, NURBS, or Coons patches. The variation of the coordinates of the control nodes are used to vary the shape of the body, that is, $s_i = \hat{x}_k = \Delta \hat{X}_k$, where $\hat{x}_k$ is a displacement of a control point in an x, y, or z direction. The variation $\boldsymbol{x} = \Delta \boldsymbol{X}$ of the mesh nodes is given by

$$\boldsymbol{x} = \sum_j \Phi_j(\xi) \hat{\boldsymbol{x}}_j \tag{21}$$

The design element concept can also be applied to describe parameter distributions and their variation in the optimization process.[27,28]

The mechanical approach has the advantage that no additional discretization besides the structure or the flow domain is necessary. However, it can be computationally expensive because, for each optimization variable, the response of a fictitious structure must be determined and the variable shape can hardly be controlled. Restricting shape variations is often necessary to guarantee smoothness or to meet geometric constraints. On the other hand, shape variations can be easily controlled in the geometrical approach by restricting the motion of the control nodes. However, in that case an additional discretization model must be generated for the design elements.

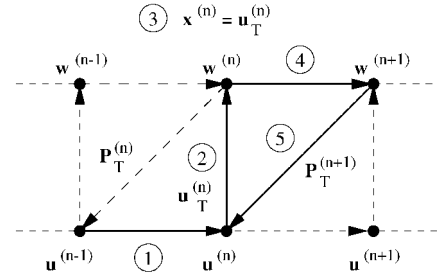

Fig. 1 Staggered algorithm for the computation of the aeroelastic steady state.

III. Aeroelastic Analysis

To predict the aeroelastic response of the system to be optimized, we couple a three-dimensional, second-order finite volume Euler code designed for flow computations on moving grids, with a general purpose finite element structural code. We base the coupling on the three-field formulation of Farhat et al.,[29] whose discrete form for steady state can be written as follows:

$$\mathcal{S}(\boldsymbol{s}, \boldsymbol{u}, \boldsymbol{x}, \boldsymbol{w}) = \boldsymbol{0} \tag{22}$$

$$\mathcal{D}(\boldsymbol{s}, \boldsymbol{u}, \boldsymbol{x}) = \boldsymbol{0} \tag{23}$$

$$\mathcal{F}(\boldsymbol{s}, \boldsymbol{x}, \boldsymbol{w}) = \boldsymbol{0} \tag{24}$$

where $\mathcal{S}$ is the state equation of the structure and can be written as

$$\mathcal{S} = \boldsymbol{K}\boldsymbol{u} - \boldsymbol{P}(\boldsymbol{x}, \boldsymbol{w}) \tag{25}$$

where $\boldsymbol{K}$ is the finite element stiffness matrix associated with the structure and $\boldsymbol{P}$ is the external load vector that combines the aerodynamic load $\boldsymbol{P}_T$ transferred from the fluid to the structure and other specified structural loads such as gravity denoted here by $\boldsymbol{P}_0$,

$$\boldsymbol{P} = \boldsymbol{P}_0 + \boldsymbol{P}_T \tag{26}$$

Equation (23) governs the motion of the fluid mesh and can be expressed as

$$\mathcal{D} = \bar{\boldsymbol{K}}\boldsymbol{x} \qquad \text{with} \qquad \boldsymbol{x} = \boldsymbol{u} \quad \text{on} \quad \Gamma_{F/S} \tag{27}$$

where $\Gamma_{F/S}$ is the interface between the fluid and the structure, $\bar{\boldsymbol{K}}$ is the fictitious stiffness matrix associated with the fluid grid and constructed according to the improved spring analogy method described by Farhat et al.,[30] and $\boldsymbol{x}$ is the motion of the fluid grid. Finally, $\mathcal{F}$ is the state equation of the fluid and can be expressed as

$$\mathcal{F} = \boldsymbol{F}_2(\boldsymbol{x}, \boldsymbol{w}) \tag{28}$$

where $\boldsymbol{F}_2$ denotes the vector of arbitrary Lagrangian Eulerian Roe fluxes resulting from a second-order finite volume discretization of the Euler flow equations.

The three-field formulation outlined earlier leads to a computational strategy that is in general 25% more computationally expensive than a comparable computational method based on a two-field formulation $(\boldsymbol{u}, \boldsymbol{w})$ of the aeroelastic problem. However, most if not all two-field formulations of computational aeroelasticity assume, among other things, a very small displacement field for the structure and, therefore, are restricted to few applications.

The three-way coupled system of Eqs. (22–24) can be solved efficiently by an iterative staggered procedure that allows the usage of three different solvers, each tailored to each different subproblem (for example, see Farhat and Lesoinne[31]). In this work, we employ the second-order staggered algorithm described next and graphically shown in Fig. 1, where the superscript (n) denotes the iteration number.

1) For a given external load $\boldsymbol{P}^{(n)}$, determine the structural response $\boldsymbol{u}^{(n)}$ by solving Eq. (25). Then, for numerical stability purposes, perform the following underrelaxation:

$$\boldsymbol{u}^{(n)} = (1 - \theta)\boldsymbol{u}^{(n-1)} + \theta \tilde{\boldsymbol{u}} \tag{29}$$

where

$$\tilde{\boldsymbol{u}} = \boldsymbol{K}^{-1}\boldsymbol{P}^{(n)}$$

and $0.5 \leq \theta \leq 0.9$ is the relaxation factor.

2) Transfer the motion of the wet surface of the structure to the fluid system $\boldsymbol{u}^{(n)} \rightarrow \boldsymbol{u}_T^{(n)}$. The general relation between $\boldsymbol{u}_T^{(n)}$ and $\boldsymbol{u}^{(n)}$ can be written as

$$\boldsymbol{u}_T^{(n)} = \boldsymbol{T}_u\, \boldsymbol{u}^{(n)} \tag{30}$$

where $\boldsymbol{T}_u$ is a transfer matrix that accounts for potentially nonmatching fluid and structure meshes (for example, see Maman and Farhat[32]).

3) Update the motion of the fluid mesh by solving Eq. (27):

$$\bar{\boldsymbol{K}}\, \boldsymbol{x}^{(n)} = 0 \qquad \text{with} \qquad \boldsymbol{x}^{(n)} = \boldsymbol{u}_T^{(n)} \quad \text{on} \quad \Gamma_{F/S} \tag{31}$$

The Dirichlet boundary conditions are introduced into the system of linear equations by partitioning $\bar{\boldsymbol{K}}$ and $\boldsymbol{x}$ as

$$\bar{\boldsymbol{K}} = \begin{bmatrix} \bar{\boldsymbol{K}}_{\Omega\Omega} & \bar{\boldsymbol{K}}_{\Omega\Gamma} \\ \bar{\boldsymbol{K}}_{\Omega\Gamma}^t & \bar{\boldsymbol{K}}_{\Gamma\Gamma} \end{bmatrix}, \qquad \boldsymbol{x} = \begin{bmatrix} \boldsymbol{x}_\Omega \\ \boldsymbol{x}_\Gamma \end{bmatrix} \tag{32}$$

where the subscript Γ designates the fluid grid points that are located at the interface between the structure and fluid models and the subscript Ω designates the remainder of the fluid grid points. Hence, $\boldsymbol{x}$ is updated by setting

$$\boldsymbol{x}_\Gamma^{(n)} = \boldsymbol{T}_u \boldsymbol{u}^{(n)} \tag{33}$$

and solving

$$\bar{\boldsymbol{K}}_{\Omega\Omega}\, \boldsymbol{x}_\Omega^{(n)} = -\bar{\boldsymbol{K}}_{\Omega\Gamma} \boldsymbol{T}_u \boldsymbol{u}^{(n)} \tag{34}$$

Note that the exact solution of the preceding system of equations is not required. What is needed is a valid update of the mesh motion $\boldsymbol{x}_\Omega^{(n)}$, that is, a mesh motion that does not produce crossovers, which can be obtained by applying a few preconditioned conjugate gradient (PCG) iterations to Eq. (34).

4) Compute the new fluid state vector $\boldsymbol{w}^{(n+1)}$ by applying a single Newton–Raphson subiteration of a defect-correction method to Eq. (24). This leads to

$$\boldsymbol{F}_2\big(\boldsymbol{w}^{(n)}\big) + \boldsymbol{H}_1\big(\boldsymbol{w}^{(n+1)} - \boldsymbol{w}^{(n)}\big) = \boldsymbol{0} \tag{35}$$

where

$$\boldsymbol{H}_1 = \frac{\partial \boldsymbol{F}_1}{\partial \boldsymbol{w}} \tag{36}$$

is the Jacobian of the first-order Roe flux. Here, the usage of $\boldsymbol{H}_1$ rather than $\boldsymbol{H}_2$ follows the rationale of a defect-correction method (even if we advocate in this context a single Newton–Raphson subiteration) and is motivated by CPU considerations. As usual, we solve the steady-state Eq. (24) by the homotopy approach

$$\boldsymbol{A}\big[\big(\boldsymbol{w} - \boldsymbol{w}^{(n)}\big)\big/\Delta\tau^{(n)}\big] + \boldsymbol{F}_2(\boldsymbol{w}) = \boldsymbol{0} \tag{37}$$

where $\boldsymbol{A}$ is the matrix of cell volumes and $\Delta\tau^{(n)}$ is the pseudo time step and, therefore, Eq. (35) is replaced in practice by

$$\big[\big(1\big/\Delta\tau^{(n)}\big)\boldsymbol{A} + \boldsymbol{H}_1\big]\big(\boldsymbol{w}^{(n+1)} - \boldsymbol{w}^{(n)}\big) = -\boldsymbol{F}_2\big(\boldsymbol{w}^{(n)}\big) \tag{38}$$

5) Extract the fluid pressure $\boldsymbol{p}^{(n+1)}$ on the fluid/structure interface $\Gamma_{F/S}$, compute the aerodynamic load $\boldsymbol{P}_F^{(n+1)}$ by integrating the fluid pressure on $\Gamma_{F/S}$, and transfer the following load to the structure:

$$\boldsymbol{P}_T^{(n+1)} = \boldsymbol{T}_p\, \boldsymbol{P}_F^{(n+1)} \tag{39}$$

where $\boldsymbol{T}_p$ is a transformation matrix that accounts for potentially nonmatching fluid and structure meshes. Here, $\boldsymbol{T}_p$ is constructed according to the conservative load transfer algorithm described by Maman and Farhat[32] and, therefore, satisfies

$$\boldsymbol{T}_p = \boldsymbol{T}_u^t \tag{40}$$

The preceding staggered algorithm can be described as a block Gauss–Seidel method. In the first optimization step, it starts from a steady-state flow around a frozen configuration of the structure. In the subsequent aeroelastic analyses within the optimization process, it starts from the aeroelastic solution of the previous design. We monitor its convergence by monitoring the relative residuals of the structure and fluid subproblems and requiring simultaneously

$$\big\|\mathcal{S}\big(\boldsymbol{s}, \boldsymbol{u}^{(n+1)}, \boldsymbol{x}^{(n+1)}, \boldsymbol{w}^{(n+1)}\big)\big\|_2 \leq \epsilon^{\mathrm{AA}} \big\|\mathcal{S}\big(\boldsymbol{s}, \boldsymbol{u}^{(0)}, \boldsymbol{x}^{(0)}, \boldsymbol{w}^{(0)}\big)\big\|_2 \tag{41}$$

$$\big\|\mathcal{F}\big(\boldsymbol{s}, \boldsymbol{x}^{(n)}, \boldsymbol{w}^{(n)}\big)\big\|_2 \leq \epsilon^{\mathrm{AA}} \big\|\mathcal{F}\big(\boldsymbol{s}, \boldsymbol{x}^{(0)}, \boldsymbol{w}^{(0)}\big)\big\|_2 \tag{42}$$

where ϵ^{AA} is a specified tolerance, where AA is aeroelastic analysis. Note that only the first inequality (41) assesses the convergence of the proposed staggered procedure. The second inequality (42) emphasizes the importance of requiring that the flow solver converges to the same precision as that imposed on the staggered algorithm.

IV. Sensitivity Analysis

The crux of the proposed aeroelastic optimization methodology, as well as a main contribution of this paper, is an accurate and affordable sensitivity analysis. Indeed, coupled nonlinear (in the sense of a nonlinear fluid model) aeroelastic sensitivity analysis remains today a computationally challenging task, particularly for large-scale computational models.

Our approach is based on the abstract framework presented by Sobieszczanski-Sobieski[33] for deriving the global sensitivity equation (GSE) of coupled systems. Our main contribution, is the specification of this approach to the three-field formulation (22–24) of the aeroelastic problem, the handling of nonconforming discrete interfaces between the structure and fluid models, the design of a fast and practical GSE solver, and the demonstration of the potential and feasibility of this technology for realistic problems.

The derivative of the optimization criterion q_j with respect to the optimization variable s_i can be computed as follows:

$$\frac{\mathrm{d}q_j}{\mathrm{d}s_i} = \frac{\partial q_j}{\partial s_i} + \frac{\partial q_j^t}{\partial \boldsymbol{u}}\frac{\mathrm{d}\boldsymbol{u}}{\mathrm{d}s_i} + \frac{\partial q_j^t}{\partial \boldsymbol{x}}\frac{\mathrm{d}\boldsymbol{x}}{\mathrm{d}s_i} + \frac{\partial q_j^t}{\partial \boldsymbol{w}}\frac{\mathrm{d}\boldsymbol{w}}{\mathrm{d}s_i} \tag{43}$$

The partial derivatives $\partial q_j/\partial s_i$, $\partial q_j/\partial \boldsymbol{u}$, $\partial q_j/\partial \boldsymbol{x}$, and $\partial q_j/\partial \boldsymbol{w}$ can be directly evaluated within the discretized structural and fluid models by taking into account the relation between the structural/aerodynamic design parameters and the abstract optimization variables defined in the design model. To determine the derivatives $\mathrm{d}\boldsymbol{u}/\mathrm{d}s_i$, $\mathrm{d}\boldsymbol{x}/\mathrm{d}s_i$, and $\mathrm{d}\boldsymbol{w}/\mathrm{d}s_i$ of the aeroelastic response with respect to the abstract variable s_i, the governing aeroelastic equations (22–24) have to be differentiated, which yields

$$\begin{bmatrix} \dfrac{\partial \mathcal{S}}{\partial s_i} \\ \dfrac{\partial \mathcal{D}}{\partial s_i} \\ \dfrac{\partial \mathcal{F}}{\partial s_i} \end{bmatrix} + \underbrace{\begin{bmatrix} \dfrac{\partial \mathcal{S}}{\partial \boldsymbol{u}} & \dfrac{\partial \mathcal{S}}{\partial \boldsymbol{x}} & \dfrac{\partial \mathcal{S}}{\partial \boldsymbol{w}} \\ \dfrac{\partial \mathcal{D}}{\partial \boldsymbol{u}} & \dfrac{\partial \mathcal{D}}{\partial \boldsymbol{x}} & \boldsymbol{0} \\ \boldsymbol{0} & \dfrac{\partial \mathcal{F}}{\partial \boldsymbol{x}} & \dfrac{\partial \mathcal{F}}{\partial \boldsymbol{w}} \end{bmatrix}}_{\mathcal{A}} \begin{bmatrix} \dfrac{\mathrm{d}\boldsymbol{u}}{\mathrm{d}s_i} \\ \dfrac{\mathrm{d}\boldsymbol{x}}{\mathrm{d}s_i} \\ \dfrac{\mathrm{d}\boldsymbol{w}}{\mathrm{d}s_i} \end{bmatrix} = \boldsymbol{0} \tag{44}$$

Again, $\partial \mathcal{S}/\partial s_i$ and $\partial \mathcal{F}/\partial s_i$ can be directly evaluated within the discretized structural and fluid models by taking into account the relation between the structural/aerodynamic design parameters and the abstract optimization variables defined in the design model. In the sequel, we denote by $\mathcal{A}$ the Jacobian of the aeroelastic problem.

To determine the gradients of the design criterion q_j with respect to the abstract optimization variable s_i, the governing equations

for the gradients of the aeroelastic response (44) are manipulated together with Eq. (43) to obtain

$$\frac{\mathrm{d}q_j}{\mathrm{d}s_i} = \frac{\partial q_j}{\partial s_i} - \begin{bmatrix} \dfrac{\partial q_j}{\partial \boldsymbol{u}} \\ \dfrac{\partial q_j}{\partial \boldsymbol{x}} \\ \dfrac{\partial q_j}{\partial \boldsymbol{w}} \end{bmatrix}^t \mathcal{A}^{-1} \begin{bmatrix} \dfrac{\partial \mathcal{S}}{\partial s_i} \\ \dfrac{\partial \mathcal{D}}{\partial s_i} \\ \dfrac{\partial \mathcal{F}}{\partial s_i} \end{bmatrix} \tag{45}$$

Equation (45) suggests two alternatives for computing the sought-after sensitivities. In the direct approach, the derivatives of the aeroelastic response are first computed for each abstract optimization variable s_i as follows:

$$\begin{bmatrix} \dfrac{\mathrm{d}\boldsymbol{u}}{\mathrm{d}s_i} \\ \dfrac{\mathrm{d}\boldsymbol{x}}{\mathrm{d}s_i} \\ \dfrac{\mathrm{d}\boldsymbol{w}}{\mathrm{d}s_i} \end{bmatrix} = -\mathcal{A}^{-1} \begin{bmatrix} \dfrac{\partial \mathcal{S}}{\partial s_i} \\ \dfrac{\partial \mathcal{D}}{\partial s_i} \\ \dfrac{\partial \mathcal{F}}{\partial s_i} \end{bmatrix} \tag{46}$$

and then substituted in Eq. (43). However, if the number of optimization criteria is smaller than the number of abstract optimization variables, it is more computationally efficient to adopt the adjoint method where the adjoint solutions

$$\boldsymbol{a}_j = \{\boldsymbol{a}_u, \boldsymbol{a}_x, \boldsymbol{a}_w\}_j$$

are computed first for each optimization criterion q_j as follows:

$$\begin{bmatrix} \boldsymbol{a}_u \\ \boldsymbol{a}_x \\ \boldsymbol{a}_w \end{bmatrix}_j = \mathcal{A}^{-T} \begin{bmatrix} \dfrac{\partial q_j}{\partial \boldsymbol{u}} \\ \dfrac{\partial q_j}{\partial \boldsymbol{x}} \\ \dfrac{\partial q_j}{\partial \boldsymbol{w}} \end{bmatrix} \tag{47}$$

Then, these adjoint solutions are injected in Eq. (45) to obtain

$$\frac{\partial q_j}{\partial s_i} = \frac{\partial q_j}{\partial s_i} - \begin{bmatrix} \boldsymbol{a}_u \\ \boldsymbol{a}_x \\ \boldsymbol{a}_w \end{bmatrix}_j^t \begin{bmatrix} \dfrac{\partial \mathcal{S}}{\partial s_i} \\ \dfrac{\partial \mathcal{D}}{\partial s_i} \\ \dfrac{\partial \mathcal{F}}{\partial s_i} \end{bmatrix} \tag{48}$$

Hence, whether the direct or adjoint approach is selected, a coupled system of linear equations has to be solved. Because of space limitations, we discuss next only the direct approach. For the adjoint approach, we refer the reader to the companion paper[34] for some preliminary results.

A. Direct Approach

From Eqs. (25–27) and (32–35), it follows that

$$\mathcal{A} = \begin{bmatrix} \boldsymbol{K} & -\dfrac{\partial \boldsymbol{P}_T}{\partial \boldsymbol{x}} & -\dfrac{\partial \boldsymbol{P}_T}{\partial \boldsymbol{w}} \\ \begin{bmatrix} \bar{\boldsymbol{K}}_{\Omega\Gamma}\boldsymbol{T}_u \\ -\boldsymbol{T}_u \end{bmatrix} & \begin{bmatrix} \bar{\boldsymbol{K}}_{\Omega\Omega} & \boldsymbol{0} \\ \boldsymbol{0} & \boldsymbol{I} \end{bmatrix} & \boldsymbol{0} \\ \boldsymbol{0} & \dfrac{\partial \boldsymbol{F}_2}{\partial \boldsymbol{x}} & \boldsymbol{H}_2 \end{bmatrix} \tag{49}$$

where $\boldsymbol{H}_2$ is the Jacobian of the second-order Roe flux. Constructing a second-order Jacobian of the fluxes is not a trivial matter, particularly for finite volume upwind schemes.[35] However, the importance of a second-order space-accurate Jacobian for sensitivity analysis is highlighted in Sec. V.

For sensitivity analysis purposes, it is conceivable to avoid the computation of the two mesh motion related matrices $\partial \boldsymbol{P}_T/\partial \boldsymbol{x}$ and $\partial \boldsymbol{F}_2/\partial \boldsymbol{x}$ to reduce computational complexity, by replacing the mesh motion equation (23), as well as its effects by a transpiration boundary condition, and reformulating the aeroelastic sensitivity problem as a standard two-field ($\mathrm{d}\boldsymbol{u}/\mathrm{d}s_i$, $\mathrm{d}\boldsymbol{w}/\mathrm{d}s_i$) problem.[36] The consequences of a related approach are investigated in Sec. V. Alternatively, we propose next another block Gauss–Seidel-like staggered solution procedure for solving the complete GSE (44) where $\partial \boldsymbol{P}_T/\partial \boldsymbol{x}$ and $\partial \boldsymbol{F}_2/\partial \boldsymbol{x}$ need not be explicitly computed and stored. Indeed, in the iterative staggered algorithm to be described, these quantities appear only in a matrix–vector product of the form $\mathcal{A}[\mathrm{d}\boldsymbol{u}/\mathrm{d}s_i \;\; \mathrm{d}\boldsymbol{x}/\mathrm{d}s_i \;\; \mathrm{d}\boldsymbol{w}/\mathrm{d}s_i]^t$. More specifically, $\partial \boldsymbol{P}_T/\partial \boldsymbol{x}$ appears and is transformed in such a matrix–vector product as follows:

$$\boldsymbol{K}\frac{\mathrm{d}\boldsymbol{u}}{\mathrm{d}s_i} - \frac{\partial \boldsymbol{P}_T}{\partial \boldsymbol{x}}\frac{\mathrm{d}\boldsymbol{x}}{\mathrm{d}s_i} - \frac{\partial \boldsymbol{P}_T}{\partial \boldsymbol{w}}\frac{\mathrm{d}\boldsymbol{w}}{\mathrm{d}s_i} = \boldsymbol{K}\frac{\mathrm{d}\boldsymbol{u}}{\mathrm{d}s_i} - \frac{\partial \boldsymbol{P}_T}{\partial s_i} \tag{50}$$

and $\partial \boldsymbol{F}_2/\partial \boldsymbol{x}$ appears in such a matrix–vector product as follows:

$$\frac{\partial \boldsymbol{F}_2}{\partial \boldsymbol{x}}\frac{\mathrm{d}\boldsymbol{x}}{\mathrm{d}s_i} + \boldsymbol{H}_2\frac{\mathrm{d}\boldsymbol{w}}{\mathrm{d}s_i} \tag{51}$$

with the advantage that $\partial \boldsymbol{P}_T/\partial \boldsymbol{x} \times \mathrm{d}\boldsymbol{x}/\mathrm{d}s_i$, $\partial \boldsymbol{P}_T/\partial \boldsymbol{w} \times \mathrm{d}\boldsymbol{w}/\mathrm{d}s_i$, and $\partial \boldsymbol{F}_2/\partial \boldsymbol{x} \times \mathrm{d}\boldsymbol{x}/\mathrm{d}s_i$ can be computed analytically in the discrete fluid model.

Let $\boldsymbol{u}$ denote the displacement of the structure at equilibrium, and as before, the superscript (n) denote the nth iteration step. The staggered algorithm we propose for solving the three-field GSE (44) with $\mathcal{A}$ given by Eq. (49) is as follows:

1) For a given derivative $\partial \boldsymbol{P}_T^{(n)}/\partial s_i$, compute the corresponding derivative of the structural displacement by differentiating Eqs. (22) and (25) and applying an underrelaxation to the obtained result. This gives

$$\frac{\mathrm{d}\boldsymbol{u}^{(n)}}{\mathrm{d}s_i} = (1-\theta)\frac{\mathrm{d}\boldsymbol{u}^{(n-1)}}{\mathrm{d}s_i} + \theta\frac{\mathrm{d}\bar{\boldsymbol{u}}}{\mathrm{d}s_i} \tag{52}$$

where $\bar{\boldsymbol{u}}$ is obtained from the solution of

$$\boldsymbol{K}\frac{\mathrm{d}\bar{\boldsymbol{u}}}{\mathrm{d}s_i} = \frac{\partial \boldsymbol{P}_0}{\partial s_i} + \frac{\partial \boldsymbol{P}_T^{(n)}}{\partial s_i} - \frac{\partial \boldsymbol{K}}{\partial s_i}\boldsymbol{u} \tag{53}$$

2) Compute

$$\frac{\mathrm{d}\boldsymbol{u}_T^{(n)}}{\mathrm{d}s_i} = \boldsymbol{T}_u\frac{\mathrm{d}\boldsymbol{u}^{(n)}}{\mathrm{d}s_i} \tag{54}$$

3) When by use of Eq. (30). Equation (31) is used and it is noted that, by construction, the fictitious stiffness matrix $\bar{\boldsymbol{K}}$ does not depend on the abstract optimization variables s_i, compute the derivative of the fluid mesh motion $\mathrm{d}\boldsymbol{x}_\Omega^{(n)}/\mathrm{d}s_i$ by solving

$$\bar{\boldsymbol{K}}_{\Omega\Omega}\frac{\mathrm{d}\boldsymbol{x}_\Omega^{(n)}}{\mathrm{d}s_i} = -\bar{\boldsymbol{K}}_{\Omega\Gamma}\frac{\mathrm{d}\boldsymbol{x}_\Gamma^{(n)}}{\mathrm{d}s_i} \tag{55}$$

with

$$\frac{\mathrm{d}\boldsymbol{x}_\Gamma^{(n)}}{\mathrm{d}s_i} = \frac{\mathrm{d}\boldsymbol{u}_T^{(n)}}{\mathrm{d}s_i}, \qquad \boldsymbol{x}^{(n)} = \boldsymbol{u}_T^{(n)} \qquad \text{on} \qquad \Gamma_{\mathrm{F/S}} \tag{56}$$

The details of this step are similar to those of step 3 of the staggered algorithm described in Sec. III.

4) By the use of Eq. (38), compute the derivatives of the fluid state variables $\mathrm{d}\boldsymbol{w}^{(n)}/\mathrm{d}s_i$ by solving

$$\boldsymbol{H}_2\frac{\mathrm{d}\boldsymbol{w}^{(n+1)}}{\mathrm{d}s_i} = -\frac{\partial \boldsymbol{F}_2}{\partial s_i} - \frac{\partial \boldsymbol{F}_2}{\partial \boldsymbol{x}}\frac{\mathrm{d}\boldsymbol{x}^{(n)}}{\mathrm{d}s_i} \tag{57}$$

5) Compute $\partial \boldsymbol{P}_F^{(n+1)}/\partial \boldsymbol{x}$ and $\partial \boldsymbol{P}_F^{(n+1)}/\partial \boldsymbol{w}$ analytically, evaluate $\partial \boldsymbol{P}_F^{(n+1)}/\partial s_i$ using the chain rule

$$\frac{\partial \boldsymbol{P}_F^{(n+1)}}{\partial s_i} = \frac{\partial \boldsymbol{P}_F^{(n+1)}}{\partial \boldsymbol{x}}\frac{\mathrm{d}\boldsymbol{x}^{(n)}}{\mathrm{d}s_i} + \frac{\partial \boldsymbol{P}_F^{(n+1)}}{\partial \boldsymbol{w}}\frac{\mathrm{d}\boldsymbol{w}^{(n)}}{\mathrm{d}s_i} \tag{58}$$

and compute

$$\frac{\partial \boldsymbol{P}_T^{(n+1)}}{\partial s_i} = \boldsymbol{T}_p\frac{\partial \boldsymbol{P}_F^{(n+1)}}{\partial s_i} \tag{59}$$

As in the case of the staggered algorithm proposed for solving the governing aeroelastic state equations, we monitor the convergence of the staggered procedure just described by requiring simultaneously

$$\left\| \boldsymbol{K}\frac{\mathrm{d}\bar{\boldsymbol{u}}^{(n+1)}}{\mathrm{d}s_i} - \frac{\partial \boldsymbol{P}_0}{\partial s_i} - \frac{\partial \boldsymbol{P}_T^{(n+1)}}{\partial s_i} + \frac{\partial \boldsymbol{K}}{\partial s_i}\boldsymbol{u} \right\|_2 \leq \epsilon^{\mathrm{SA}} \left\| \boldsymbol{K}\frac{\mathrm{d}\bar{\boldsymbol{u}}^{(0)}}{\mathrm{d}s_i} - \frac{\partial \boldsymbol{P}_0}{\partial s_i} - \frac{\partial \boldsymbol{P}_T^{(0)}}{\partial s_i} + \frac{\partial \boldsymbol{K}}{\partial s_i}\boldsymbol{u} \right\|_2 \tag{60}$$

$$\left\| \boldsymbol{H}_2\frac{\mathrm{d}\boldsymbol{w}^{(n+1)}}{\mathrm{d}s_i} + \frac{\partial \boldsymbol{F}_2}{\partial s_i} + \frac{\partial \boldsymbol{F}_2}{\partial \boldsymbol{x}}\frac{\mathrm{d}\boldsymbol{x}}{\mathrm{d}s_i}^{(n+1)} \right\|_2 \leq \epsilon^{\mathrm{SA}} \left\| \boldsymbol{H}_2\frac{\mathrm{d}\boldsymbol{w}}{\mathrm{d}s_i}^{(0)} + \frac{\partial \boldsymbol{F}_2}{\partial s_i} + \frac{\partial \boldsymbol{F}_2}{\partial \boldsymbol{x}}\frac{\mathrm{d}\boldsymbol{x}}{\mathrm{d}s_i}^{(0)} \right\|_2 \tag{61}$$

where ϵ^{SA} is a specified tolerance and SA is sensitivity analysis. Again, note that only the first inequality (60) assesses the convergence of the proposed staggered procedure. The second inequality (61) emphasizes the importance of requiring that the flow solver converges to the same precision as that imposed on the staggered algorithm.

Finally, we note that the convergence of the preceding iterative staggered procedure proposed herein for solving the GSE (44) can be accelerated by storing at a given optimization step the gradients of the fluid state, and using these to initialize the sensitivity analysis in the following optimization step. Such a technique increases the memory requirements but accelerates the solution time.

V. Applications and Numerical Investigations

In this section, we first illustrate the aeroelastic sensitivity analysis presented in this paper and investigate some interesting computational issues. Then, we highlight the potential of the proposed aeroelastic optimization methodology by applying it to one academic and one realistic wing problem. In all cases, we solve all fluid subproblems such as Eqs. (38) and (57) by a parallel generalized minimum residual (GMRES) algorithm preconditioned by a restricted additive Schwarz method (see Cai et al.[37]) and all structural subproblems such as (1) and (53) by a direct method. We perform all computations in double-precision arithmetic on a 12-processor Origin 2000 system.

A. Aeroelastic Sensitivity Analysis of an Idealized Wing Structure

Besides illustrating the proposed aeroelastic sensitivity method, our objective here is to investigate the influence of the following parameters on accuracy and computational efficiency, that is, on performance: 1) mesh refinement, 2) order of accuracy of the Jacobian $\boldsymbol{H}$ used in the sensitivity analysis, and 3) degree to which the effect of the mesh motion is included in the sensitivity analysis.

For this purpose, we consider a cantilevered wing with a NACA0012 airfoil. We idealize the structure as a flat plate and assume that it is made of an isotropic material characterized by Young's modulus $E = 1.45 \times 10^{11}$ N/m^2 and Poisson ratio $\nu = 0.2$ and that its thickness is $th = 0.025$ m. We set the angles of attack to $\alpha = 2.5$ deg (pitch), and $\beta = 0$ deg (yaw), the freestream Mach number to $M_\infty = 0.6$, and the remaining freestream flow conditions to those corresponding to a flight at an altitude of 10,000 m ($\rho_\infty = 4.135 \times 10^{-1}$ kg/m^3 and $p_\infty = 2.650 \times 10^4$ N/m^2). We discretize the flat plate by 768 three-noded shell elements and the fluid computational domain by 44,598 grid points (Fig. 2). We label this specific fluid mesh as mesh A and note that the structure mesh and the fluid mesh on the wet surface do not match geometrically and topologically.

In all computations aimed at investigating the effect of mesh refinement, we set $\epsilon^{\mathrm{AA}} = \epsilon^{\mathrm{SA}} = 10^{-8}$. For these computations, we choose this rather small value for the tolerances to guard our conclusions against any effect of algebraic misconvergence. On the other hand, in all computations aimed at assessing the effect on performance of the order of accuracy of the Jacobian $\boldsymbol{H}$ and/or the degree to which the mesh motion is accounted for in the sensitivity analysis, we set $\epsilon^{\mathrm{AA}} = \epsilon^{\mathrm{SA}} = 10^{-5}$.

First, we compute the sensitivity of each of the drag, lift, and von Mises stress σ_E on the upper surface of the plate at point E, and of vertical displacement of the plate u_C at point C, with respect to the structural thickness, s_1, the backsweep of the wing, s_2, the freestream Mach number, s_3, and the α angle of attack, s_4. For controlling the variation of the backsweep, we adopt the design element concept outlined in Sec. II.B. More specifically, we describe the geometry of the structural model by a single Coons element A–B–C–D with linear shape functions along the edges. We identify varying the backsweep with varying the horizontal position of the control nodes C and D and, therefore, define the abstract optimization variable s_2 as $s_2 = \hat{x}_1^C = \hat{x}_1^D$. Each value of s_2 defines a unique structural shape variation that must be superposed to the elastic displacement field $\boldsymbol{u}$ before performing Eq. (33) and solving Eq. (34) to update the motion $\boldsymbol{x}$ of the fluid mesh.

We report in Table 1 the obtained aeroelastic sensitivity results. Note that all of the sensitivities with respect to the angle of attack α are given in per radian. The sensitivities in Table 1 reflect well-known effects, such as increasing the backsweep decreases the drag, increasing the Mach number increases the lift, and increasing the structural thickness decreases the stress level.

1. *Effect of Mesh Refinement*

For a flat plate structure, the finite element model described earlier is sufficiently well resolved. Therefore, we consider here refining the fluid mesh only, and construct mesh C with 87,827 grid points. For comparison purposes, we also generate a coarser mesh than mesh A, namely, mesh B with 19,384 grid points. We report in Table 2 the relative variations of the earlier computed sensitivities with the size of the fluid mesh.

The results reported in Table 2 show that only the accurate prediction of the drag requires a finer mesh than mesh A. The aerodynamic lift, the structural displacement u_C, as well as their sensitivities with respect to the thickness, backsweep, and angle of attack α, are well converged for mesh A, and the sensitivities of the structural displacement u_C and the von Mises stress σ_E with respect to the backsweep and the Mach number are reasonably well converged.

2. *Approximate Sensitivities*

There are two tempting approaches for reducing the computational complexity of the proposed sensitivity analysis and, therefore,

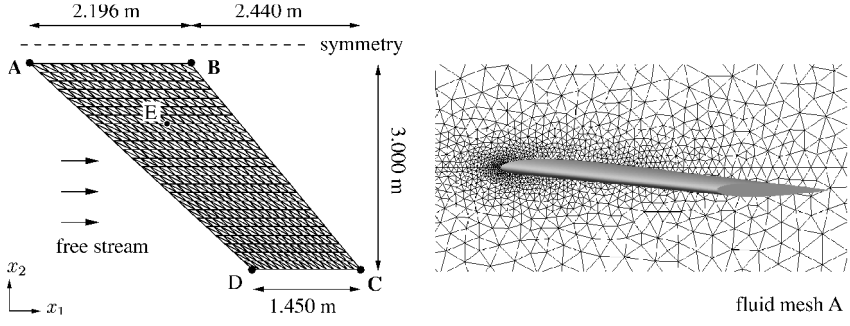

Fig. 2 Discretization of the idealized wing structure and surrounding flow.

Table 1 Aeroelastic sensitivity analysis

Approach	Drag, N	Lift, N	Stress σ_E, N/m^2	Displacement u_C, m
Aeroelastic analysis	184.027	5218.84	1.9018×10^7	0.07701
Sensitivity analysis optimization variables				
Thickness, m	2471.78	76450.8	-1.1454×10^9	−7.74288
Backsweep, m	−50.0883	−1026.39	2.6455×10^6	0.02677
Mach number	582.253	19263.4	5.7221×10^6	0.02318
Angle of attack α, rad	3616.88	119157.1	4.3586×10^8	1.76462

Table 2 Relative variations of the aerodynamic and structural criteria as well as their sensitivities with the size of the fluid mesh[a]

Approach	Δ drag, %		Δ lift, %		Δ stress σ_E, %		Δ displacement, u_C %	
Aeroelastic analysis	51.50	|−26.49	−1.32	|0.43	−0.87	|0.50	−0.80	|0.40
Sensitivity analysis optimization variables								
Thickness	4.89	| −3.95	−0.29	|0.54	−1.35	|0.48	−1.14	|0.39
Backsweep	29.90	|−18.22	−0.00	|0.19	−4.60	|1.95	−2.26	|1.11
Mach number	40.27	|−20.54	−1.47	|0.34	−2.30	|1.66	−7.07	|0.57
Angle of attack α	0.60	| −0.91	−0.93	|0.77	−0.24	|0.91	0.01	|0.83

[a]Format is mesh B| mesh C, and reference values are those tabulated in Table 1 for mesh A.

Table 3 Relative errors in the sensitivities associated with the simplified computational strategies

	Relative errors in the sensitivities, %		
Sensitivity variable	SH1	SH2SM	SH1SM
Lift with respect to thickness	4.94	14.66	13.29
Lift with respect to backsweep	3.05	0.93	67.62
Displacement with respect to thickness	3.29	6.07	2.48
Displacement with respect to backsweep	12.25	8.80	69.80

Table 4 Performance of the aeroelastic sensitivity analysis using four different computational strategies

	Approach			
Computational cost	SH2	SH1	SH2SM	SH1SM
Total no. of iterations				
Staggered procedure (52–59)	15	14	14	15
GMRES (57)	317	271	255	262
PCG (55)	246	220	0	0
CPU time, s				
Overall	235	220	143	148
Mesh motion	61	57	0	0

increasing the speed of the optimization process. The first one consists in employing the first-order flux Jacobian $\boldsymbol{H}_1$ instead of the second-order one $\boldsymbol{H}_2$ in Eq. (49) because $\boldsymbol{H}_1$ is computationally cheaper to evaluate than $\boldsymbol{H}_2$. The second one consists in setting $\mathrm{d}\boldsymbol{x}_\Omega/\mathrm{d}s_i = 0$ on the basis that the mesh motion of the fluid grid points that are not located on the fluid/structure interface is a mathematical artifact of the proposed sensitivity analysis methodology and perhaps does not affect its performance. Such an assumption eliminates the need to solve problem (55), which arises at each iteration of the staggered procedure proposed for solving the GSE. Both approaches, which could also be combined, amount to computing approximate sensitivities rather than sensitivities that are consistent with the three-field formulation (22–24) of the aeroelastic problem. To investigate the merit of these approaches, we consider again the wing problem described in Sec. V.A and define the following four different computational strategies: 1) SH2, using $\boldsymbol{H}_2$ in Eq. (49) and taking into account $\mathrm{d}\boldsymbol{x}_\Omega/\mathrm{d}s_i$; 2) SH1, using $\boldsymbol{H}_1$ in Eq. (49) and taking into account $\mathrm{d}\boldsymbol{x}_\Omega/\mathrm{d}s_i$; 3) SH2SM, using $\boldsymbol{H}_2$ in Eq. (49) and ignoring $\mathrm{d}\boldsymbol{x}_\Omega/\mathrm{d}s_i$ (simplified mesh motion); and 4) SH1SM, using $\boldsymbol{H}_1$ in Eq. (49) and ignoring $\mathrm{d}\boldsymbol{x}_\Omega/\mathrm{d}s_i$ (simplified mesh motion).

Note that the computational strategy SH2, which is the only one among the four that is mathematically consistent with our formulation of the aeroelastic problem, is the one used for generating the results reported in the two preceding subsections.

We adopt mesh A and recompute the same aeroelastic sensitivities as before using the four different computational strategies just outlined. Setting the results of the computational strategy SH2 as reference results, we report in Table 3 the relative errors in the sensitivities predicted by the other computational strategies. We also summarize in Table 4 the performance results obtained when the proposed aeroelastic sensitivity procedure is equipped with either of the four computational strategies.

Observe that, at least for this problem, using a first-order rather than second-order flux Jacobian in the sensitivity analysis, or setting $\mathrm{d}\boldsymbol{x}_\Omega/\mathrm{d}s_i = 0$, results in relative errors in the sensitivities that are less than 15%. However, combining both approximations leads to an unacceptable maximum error that exceeds 60%.

Also observe that, in all cases, the staggered procedure (52–59) converges in 14–15 outer iterations. Throughout these iterations, the accumulated number of GMRES iterations for solving the fluid subproblems (57) is slightly higher for the mathematically consistent strategy SH2, because this strategy generates more ill-conditioned systems. The simplified computational strategies SH2SM and SH1SM reduce significantly the CPU time, but deliver unacceptable accuracies. Both Tables 3 and 4 show that SH2 delivers the best performance/accuracy ratio. The performance results summarized in Table 4 also suggest that, for the mathematically consistent strategies for computing the gradients, handling the fluid mesh motion accounts for about 26% of the total CPU time, which is a reasonable CPU cost.

B. Aeroelastic Optimization of a Composite Wing

Next, we consider again the same wing as in Sec. V.A but idealize here the structure as a two-ply composite plate with the first layer characterized by a uniform Young modulus $E_1 = 1.45 \times 10^{11}$ N/m^2 and the second layer by $E_2 = 3.28 \times 10^9$ N/m^2. We also assume that both layers have the same shear modulus $G = 3.38 \times 10^9$ N/m^2, Poisson ratio $\nu_{12} = 0.2$, and effective thickness $th = 0.0275$ m. We discretize the idealized structure by 432 three-noded composite shell elements and the fluid computational domain by 23,298 grid points.

We consider an initial design where the fiber orientations are $\phi_1 = 0$ deg and $\phi_2 = 45$ deg with respect to the axis of symmetry of the plane and clamp again the wing at its root A–B (Fig. 2). We

seek to minimize the drag over lift ratio D/L of this wing for three different freestream Mach numbers $M_\infty = [0.4, 0.8, 1.2]$ by optimizing the orientation of its composite fibers. The other freestream flow conditions are the same as given in Sec. V.A.

We report in Table 5, for each Mach number, the predicted optimal fiber orientation and the achieved reduction in D/L as a percentage of the drag over lift ratio of the initial design.

For each considered Mach number, the optimal fiber orientations appear to be the same for both layers, which can be expected when the layers have the same geometry and thickness. In all three cases, the drag over lift ratio is reduced by increasing the lift rather than reducing the drag. Furthermore, Fig. 3 reveals that the optimal fiber orientations increase the wing bending and torsional flexibilities. This illustrates the indirect role that composite fibers can play in optimizing the deformed shape. A larger twisting leads to a higher local angle of attack α, which in turn leads to a higher induced drag and, for this problem, an even higher lift.

Table 5 Optimization results for a two-layer composite wing for different Mach numbers

	Mach number		
Design	$M_\infty = 0.4$	$M_\infty = 0.8$	$M_\infty = 1.2$
Initial			
Drag, kN	2.949	9.464	86.548
Lift, kN	24.970	117.376	202.102
Optimized			
Fiber angle ϕ_1, deg	27.78	26.67	29.55
Fiber angle ϕ_2, deg	27.78	26.67	29.71
Drag, kN	2.994	10.728	98.109
Lift, kN	25.935	140.576	315.322
Reduction of D/L, %	2.261	5.35	27.36

C. Shape and Thickness Optimization of the ARW2 Wing

Here, we illustrate the computational methodology presented in this paper with the aeroelastic optimization of the ARW2 wing,[38] whose geometry and material properties are summarized in Table 6. Unlike in the earlier examples, we consider here a detailed finite element model of the structure (Fig. 4) that includes, among others, the spars, ribs, hinges, and control surfaces of this wing, and that contains a total of 11,838 degrees of freedom. We generate a three-dimensional unstructured fluid mesh around the wet surface with 43,847 grid points.

We consider a flight configuration at 12,200 m with $\rho_\infty = 2.928 \times 10^{-1}$ kg/m^3, $p_\infty = 1.882 \times 10^4$ N/m^2, and set $M_\infty = 0.8$

Table 6 Basic structural data of the ARW2

Parameter	Value
Geometry, m	
Tip AB	0.318
Root CD	1.022
Wingspan AD	2.665
Material properties	
Skin (except flaps)	Various composite materials[38]
Stiffeners	Aluminum
E	7.1 10^{10} N/m^2
ν	0.32
ρ	2.794 10^3 kg/m^3

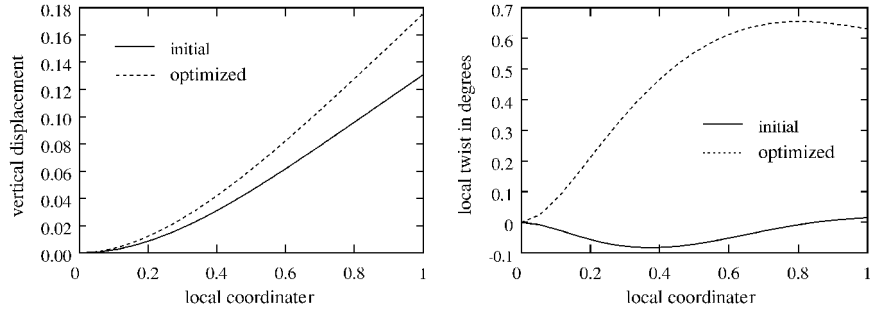

Fig. 3 Vertical displacement and local twist angle along the one-quarter chordlength line for $M_\infty = 0.8$.

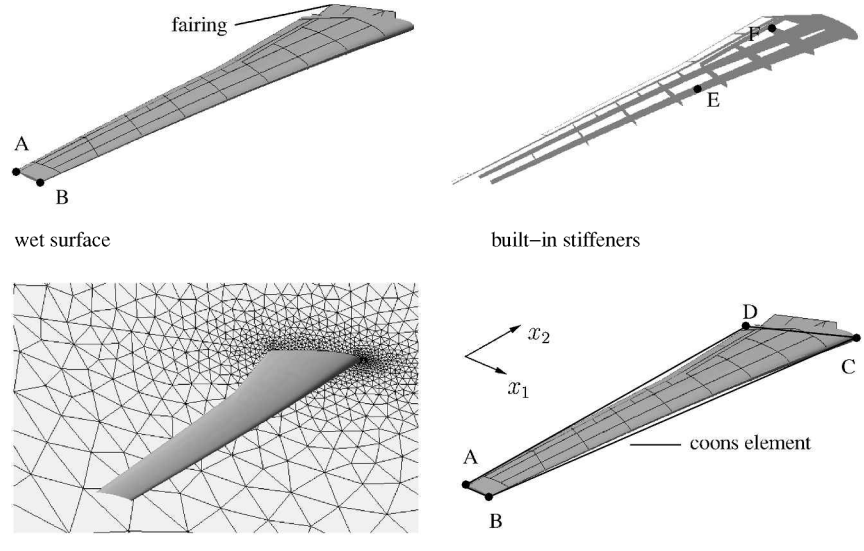

Fig. 4 ARW2 structural, fluid, and design models; initial configuration.

and the angles of attack to $\alpha = 2.5$ deg and $\beta = 0$ deg. Again, we seek to minimize the drag over lift ratio. However, for this wing problem, we introduce the following lift, stress, and displacement optimization constraints:

1) The lift L can change only by an amount greater or equal to the variation of the weight induced by the variation of the thickness of the stiffeners. We write this as follows:

$$\Delta L \geq 2\Delta W \tag{62}$$

where W is the weight of the wing and the factor 2 is to account for the weight of half of the fuselage and other supporting structures.

2) The vertical displacements at the points A and B (Fig. 4) cannot exceed $u_{\max} = 0.381$ m. This maximum displacement constraint can also be interpreted as a maximum bending flexibility constraint.

3) The von Mises stress in the stiffeners cannot exceed $\sigma_{\max} = 9.05 \times 10^7$ N/m^2. This value of $\sigma_{\max}$ is suggested by the maximum von Mises stress of 8.90×10^7 N/m^2 associated with the initial design. Because the stresses are controlled at each finite element node for the upper, middle, and lower surfaces of a plate or shell element, this leads to 2412 stress constraints.

We perform the constrained aeroelastic optimization by varying the backsweep and twisting of the wing (Fig. 5), as well as the thicknesses of its stiffeners as follows:

1) We control the shape of the wing by the design element concept. More specifically, we introduce a Coons element A–B–C–D in the ground plan x_1–x_2 of the wing (Fig. 4) and introduce the following bounded optimization variables:

$$s_1 = \hat{x}_1^A = \hat{x}_1^B, \qquad -0.635 \leq s_1 \leq 0.635 \text{ m}$$

$$s_2 = \hat{x}_2^B = -\hat{x}_2^A, \qquad -0.0254 \leq s_2 \leq 0.01016 \text{ m}$$

2) We subdivide the stiffeners into two groups. In the first group, we choose to vary the thickness as a linear function of two optimization variables s_3 and s_4 to account for the initial variations in the thickness of the stiffeners in this first group. In the second group, we identify the thickness variation with a single abstract optimization variable s_5, that is, we force all of the stiffeners to have the same thickness variation. To avoid a zero thickness stiffener, we limit s_3, s_4, and s_5 by $-0.002565 \leq s_3 \leq 0.0127$ m and $-0.000762 \leq s_4, s_5 \leq 0.0381$ m.

When the SH2 computational strategy defined in Sec. V.A for the sensitivity analysis is used, the proposed aeroelastic optimization method converges after 20 iterations to the optimal shape and thickness corrections graphically shown in Fig. 5 and reduces the drag over lift ratio, that is, the objective function, by a factor equal to 1.24 (19.44%). Table 7 contrasts some performance characteristics of the initial and optimized designs of the ARW2 wing. From these results, we conclude that, for this problem, our constrained aeroelastic optimization reduces the D/L ratio essentially by reducing the drag. It increases the backsweep, which reduces wave drag, and adjusts only slightly the twist of the wing. Figure 6, which compares the Mach contour plots of the initial and optimized configurations, also reveals that the optimized configuration features a weaker shock, which is consistent with drag

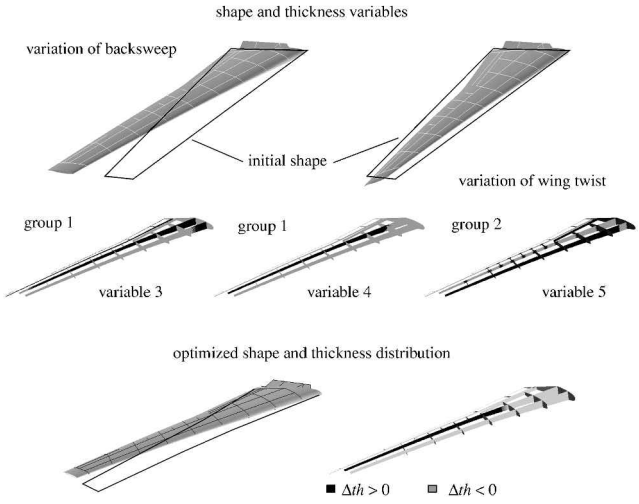

Fig. 5 Optimization variables and optimal configuration: backsweep s_1, 0.49772 m; twist s_2, 0.00347 m; Δ thickness s_3, − 0.00247 m; Δ thickness s_4, 0.00212 m; and Δ thickness s_5, − 0.00076 m.

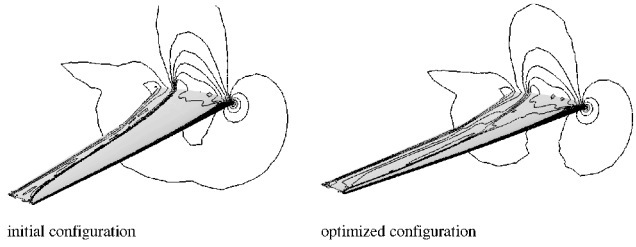

Fig. 6 Steady-state Mach contours for initial and optimized configurations.

Table 7 Aeroelastic characteristics of the initial and optimized designs of the ARW2 wing

Parameter	Configuration	
	Initial$^{(0)}$	Optimized
Lift L, N	9.63798×10^3	8.06121×10^3
Drag D, N	0.48684×10^3	0.32764×10^3
D/L	0.505	0.406
Weight of wing, N	1.78100×10^3	0.99256×10^3
Vertical displacement at point B m	0.23141	0.25284
Maximum von Mises stress, N/m^2	8.90134×10^7 (reached at point E)	9.05000×10^7 (reached at point F)

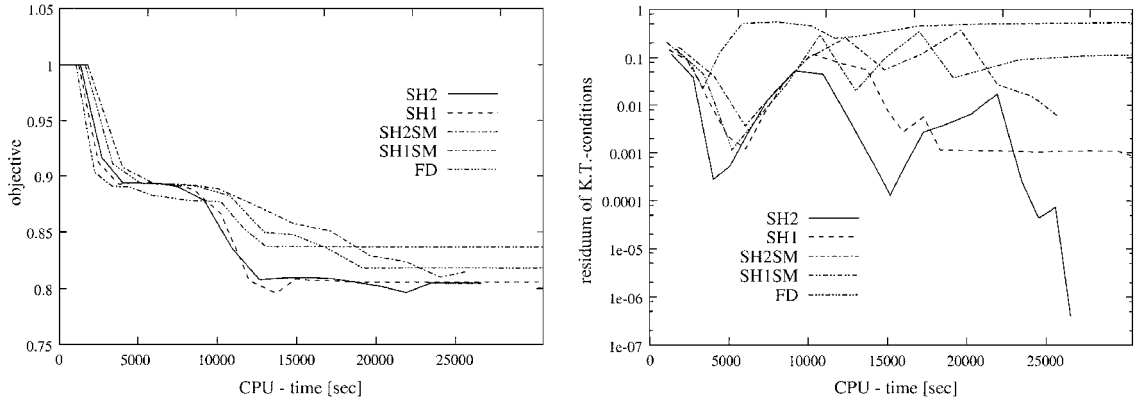

Fig. 7 Convergence of the objective function using different computational strategies for the sensitivity analysis.

reduction. The reduction of the thicknesses of some stiffeners results in a significant reduction of the weight of the wing. A comparison of the displacements and maximum stresses of the initial and optimized configurations also reveals that the optimized wing is more flexible in bending but is subjected to a slightly higher stress level.

Finally, we show in Fig. 7 the performance results obtained for our optimization methodology and this ARW2 problem, when equipped with the four different computational strategies defined in Sec. V.A, as well as a central finite difference scheme for performing the sensitivity analysis. These results confirm again that using the second-order Jacobian of the fluxes and taking into account the sensitivity of the mesh motion with respect to the abstract optimization variables in the computation of the gradients of the optimization criteria (strategy SH2) is the winning strategy. They also highlight the superiority of the analytical approach for computing the gradients over finite differencing.

VI. Conclusions

We have described a methodology for the aeroelastic optimization of realistic aircraft structures. This methodology relies on the practical as well as efficient solution by a staggered scheme of the analytically derived global sensitivity equations associated with the three-field formulation of an aeroelastic problem, as well as the fast evaluation, also by a staggered algorithm, of the aeroelastic response of each intermediate configuration. We have illustrated this methodology and highlighted its potential with the aeroelastic optimization of various idealized and builtup wing structures. All obtained performance results highlight the superior performance of a mathematically consistent evaluation of the gradients in the sensitivity analysis, that is, a second-order evaluation of the flux Jacobian when the flow is discretized by a second-order space-accurate scheme, and a proper evaluation of the sensitivities with respect to the fluid mesh motion because this mesh motion is an integral component of the three-field formulation of an aeroelastic problem. These results also point to the superior performance of the optimization loop when the gradients are based on the analytically derived global sensitivity equations rather than on finite differences.

Acknowledgments

The authors acknowledge the partial support by the National Science Foundation under Grant ECS-9725504 and the partial support by the Air Force Office of Scientific Research under Grant F49620-99-1-007. They thank K. Schittkowski for providing them with the source code of the sequential quadratic programming algorithm.

References

[1]Kirsch, U., *Structural Optimization: Fundamentals and Applications*, Springer, Berlin, 1993.

[2]Bendsøe, M., *Optimization of Structural Topology, Shape, and Material*, Springer, Berlin, 1995.

[3]Newman, P., Hou, G.-W., and Taylor, A., "Observations Regarding Use of Advanced CFD Analysis, Sensitivity Analysis, and Design Codes in MDO," *Multidisciplinary Design Optimization—State of the Art*, edited by N. Alexandrov and Y. Hussaini, Society for Industrial and Applied Mathematics, Philadelphia, 1997, pp. 263–279.

[4]Jameson, A., "Re–Engineering the Design Process through Computation," AIAA Paper 97-0641, 1997.

[5]Haftka, R., "Structural Optimization with Aeroelastic Constraints—A Survey of U.S. Applications," *International Journal of Vehicle Design*, Vol. 7, No. 3–4, 1986, pp. 381–392.

[6]Bowman, K., Grandhi, R., and Eastep, F., "Structural Optimization of Lifting Surfaces with Divergence and Control Reversal Constraints," *Structural Optimization*, Vol. 1, No. 1, 1989, pp. 153–161.

[7]Friedmann, P., "Helicopter Vibration Reduction Using Structural Optimization with Aeroelastic/Multidisciplinary Constraints: A Survey," *Journal of Aircraft*, Vol. 28, No. 1, 1991, pp. 8–21.

[8]Barthelemy, J.-F., Wrenn, G., Dovi, A., and Hall, L., "Supersonic Transport Wing Minimum Design Integrating Aerodynamics and Structures," *Journal of Aircraft*, Vol. 31, No. 2, 1994, pp. 330–338.

[9]Giunta, A., and Sobieszczanski-Sobieski, J., "Progress Toward Using Sensitivity Derivatives in a High-Fidelity Aaeroelastic Analysis of a Supersonic Transport," *Proceedings of the 7th AIAA/USAF/NASA/ISSMO Symposium on Multidisciplinary Analysis and Optimization*, AIAA, Reston, VA, 1998, pp. 441–453.

[10]Giunta, A., "Novel Sensitivity Analysis Method for High Fidelity Multidisciplinary Optimization of Aerostructural Systems," AIAA Paper 2000-0683, Jan. 2000.

[11]Ghattas, O., and Li, X., "Domain Decomposition Methods for Sensitivity Analysis of a Nonlinear Aeroelastic Problem," *International Journal of Computational Fluid Dynamics*, Vol. 11, No. 1–2, 1998, pp. 113–130.

[12]MØller, H., and Lund, E., "Shape Sensitivity Analysis of Strongly Coupled Fluid–Structure Interaction Problems," AIAA Paper 2000-4823, Sept. 2000.

[13]Maute, K., Lesoinne, M., and Farhat, C., "Optimization of Aeroelastic Systems Using Coupled Analytical Sensitivities," AIAA Paper 2000-0560, Jan. 2000.

[14]Hou, G.-W., and Satyanarayana, A., "Analytical Sensitivity Analysis of a Statical Aeroelastic Wing," AIAA Paper 2000-4824, Sept. 2000.

[15]Maute, K., Schwarz, S., and Ramm, E., "Structural Optimization—The Interaction Between Form and Mechanics," *ZAMM*, Vol. 79, No. 10, 1999, pp. 651–674.

[16]Gill, P., Murray, W., and Wright, M., *Practical Optimization*, Academic Press, London, 1981.

[17]Vanderplaats, G., *Numerical Optimization Techniques for Engineering Design: With Applications*, McGraw–Hill, New York, 1984.

[18]Schittkowski, K., Zillober, C., and Zotemantel, R., "Numerical Comparison on Nonlinear Programming Algorithms for Structural Optimization," *Structural Optimization*, Vol. 7, 1994, pp. 1–28.

[19]Schittkowski, K., "NLPQL: A FORTRAN Subroutine for Solving Constrained Nonlinear Programming Problems," *Annals of Operations Research*, Vol. 5, No. 6, 1985, pp. 485–500.

[20]Gill, P., Saunders, M., and Murray, W., "SNOPT: An SQP Algorithm for Large-Scale Constrained Optimization," Dept. of Mathematics, Rept. NA 97-2, Univ. of California, San Diego, CA, 1997.

[21]Luenberger, D., *Linear and Nonlinear Programming*, Addison Wesley Longman, Reading, MA, 1984.

[22]Zienkiewicz, O., and Campbell, J., "Shape Optimization and Sequential Linear Programming," *Optimum Structural Design*, edited by R. H. Gallagher and O. C. Zienkiewicz, Wiley, New York, 1973, pp. 109–126.

[23]Kikuchi, N., Chung, K., Torigaki, T., and Taylor, J., "Adaptive Finite Element Methods for Shape Optimization of Linearly Elastic Structures," *Computational Methods in Applied Mechanical Engineering*, Vol. 57, No. 1, 1986, pp. 67–89.

[24]Belegundu, A., and Rajan, S., "A Shape Optimization Approach Based on Natural Design Variables and Shape Functions," *Computational Methods in Applied Mechanical Engineering*, Vol. 66, No. 1, 1988, pp. 87–106.

[25]Böhm, W., Farin, G., and Kahmann, J., "A Survey of Curve and Surface Methods in CAGD," *Computer Aided Design*, Vol. 1, No. 1, 1984, pp. 1–60.

[26]Farin, G., *Curves and Surfaces for Computer Aided Geometric Design*, Academic Press, London, 1988.

[27]Bennett, J., and Botkin, M., "Structural Shape Optimization with Geometric Description and Adaptive Mesh Refinement," *AIAA Journal*, Vol. 23, No. 3, 1985, pp. 458–464.

[28]Bletzinger, K.-U., Kimmich, S., and Ramm, E., "Efficient Modeling in Shape Optimal Design," *Computing Systems in Engineering*, Vol. 2, No. 5–6, 1991, pp. 483–495.

[29]Farhat, C., Lesoinne, M., and Maman, N., "Mixed Explicit/Implicit Time Integration of Coupled Aeroelastic Problems: Three-Field Formulation, Geometric Conservation and Distributed Solution," *International Journal for Numerical Methods in Fluids*, Vol. 21, No. 10, 1995, pp. 807–835.

[30]Farhat, C., Degand, C., Koobus, B., and Lesoinne, M., "Torsional Springs for Two-Dimensional Dynamic Unstructured Fluid Meshes," *Computational Methods in Applied Mechanical Engineering*, Vol. 163, No. 1–4, 1998, pp. 231–245.

[31]Farhat, C., and Lesoinne, M., "Two Efficient Staggered Procedures for the Serial and Parallel Solution of Three-Dimensional Nonlinear Transient Aeroelastic Problems," *Computational Methods in Applied Mechanical Engineering*, Vol. 182, No. 3–4, 2000, pp. 499–515.

[32]Maman, N., and Farhat, C., "Matching Fluid and Structure Meshes for Aeroelastic Computations: A Parallel Approach," *Computers and Structures*, Vol. 54, No. 4, 1995, pp. 779–785.

[33]Sobieszczanski-Sobieski, J., "Sensitivity of Complex, Internally Coupled Systems," *AIAA Journal*, Vol. 28, No. 1, 1990, pp. 153–160.

[34]Maute, K., Nikbay, M., and Farhat, C., "Analytically Based Sensitivity Analysis and Optimization of Nonlinear Aeroelastic Systems," AIAA Paper 2000-4825, Sept. 2000.

[35] Lesoinne, M., Sarkis, M., Hetmaniuk, U., and Farhat, C., "A Linearized Method for the Frequency Analysis of Three-Dimensional Fluid/Structure Interaction Problems in All Flow Regimes," *Computer Methods in Applied Mechanics and Engineering*, Vol. 190, No. 24–25, 2001, pp. 3121–3146.

[36] Piperno, S., Farhat, C., Larrouturou, B., "Partitioned Procedures for the Transient Solution of Coupled Aeroelastic Problems," *Computational Methods in Applied Mechanical Engineering*, Vol. 124, No. 1–2, 1995, pp. 79–112.

[37] Cai, X.-C., Farhat, C., and Sarkis, M., "A Minimum Overlap Restricted Additive Schwarz Preconditioner and Applications in 3D Flow Simulations," *Tenth International Conference on Domain Decomposition Methods for Partial Differential Equations*, edited by J. Mandel, C. Farhat, and X.-C. Cai, American Mathematical Society, Providence, RI, 1998, pp. 479–485.

[38] Sandford, M., Seidel, D., Eckstrom, C., and Spain, C., "Geometrical and Structural Properties of an Aeroelastic Research Wing (ARW-2)," NASA TM-4110, 1989.

E. Livne
Associate Editor